Entanglement generation between two atoms via surface modes

Jingping Xu,[1] M. Al-Amri,[2] Yaping Yang,[1] Shi-Yao Zhu,[1,3,4] and M. Suhail Zubairy[3,5]

[1]*Key Laboratory of Advanced Micro-structure Materials, Ministry of Education, Department of Physics, Tongji University, Shanghai 200092, China*

[2]*The National Center for Mathematics and Physics, KACST, P.O. Box 6086, Riyadh 11442, Saudi Arabia*

[3]*Beijing Computational Science Research Center, Beijing 100084, China*

[4]*Department of Physics, Hong Kong Baptist University, Hong Kong, China*

[5]*Institute for Quantum Science and Engineering (IQSE) and Department of Physics and Astronomy, Texas A&M University, College Station, Texas 77843, USA*

(Received 12 July 2011; published 22 September 2011)

We discuss the coupling of two identical atoms, separated by a metal or metamaterial slab, through surface modes. We show that the coupling through the surface modes can induce entanglement. We discuss how to control the coupling for the metal or metamaterial slab by adjusting the symmetrical and antisymmetrical property of the surface modes. We analyze the dispersion relation of the surface modes and study the parameter ranges that support the surface modes with the same properties. Our results have potential applications in quantum communication and quantum computation.

DOI: 10.1103/PhysRevA.84.032334 PACS number(s): 03.67.Mn, 42.50.Nn, 42.50.Dv

I. INTRODUCTION

Generation and preservation of entanglement is an important subject in quantum information and quantum computing [1]. The vacuum fluctuations can affect the state of qubits in a number of ways. On the one hand, the vacuum fluctuations can lead to decay that can adversely affect the quantum coherence and reduce entanglement [2,3]. On the other hand, the decay due to the vacuum fluctuation can generate entanglement from initially unentangled qubits [4–10], thus leading to induced entanglement. This latter effect has been studied for identical qubits coupled to either a common multimode vacuum field [4–8] or to a damped single-mode cavity field [9,10]. Such a process has been called the delayed sudden birth of entanglement [8] as opposed to the sudden death of entanglement from an initially entangled state. Most previous studies about the sudden birth of entanglement [4–8] require two close-lying atoms with a distance less than one wave length at the transition frequency. Recently, it has been proposed to realize such entanglement generation between two distant qubits (about ten wavelengths apart) by using left-handed materials [11] via enhancement of the interaction between distant qubits. Another way to attain entanglement between atoms such that the qubit-qubit distance is larger than one operating wavelength employs the surface plasmonic mode. The entanglement of two qubits mediated by metal nanowire [12] and a one-dimensional plasmonic waveguide [13] has been studied.

With the development of techniques in quantum information, the miniaturization of practical quantum devices is an important issue. The present techniques based on semiconductor technology require us to precisely locate each qubit as well as to insulate them from each other by solid-state materials. The generation and preservation of the entanglement of qubits, as well as the insulation of qubits, are the current research frontier. In this paper, we study the entanglement of two two-level atoms separated by a slab of materials (including metal and metamaterials), which is the simplest model of a miniaturized quantum device.

The paper is organized as follows. In Sec. II, we derive the model and show the general principle of induced entanglement of two atoms. In Sec. III, we analyze the coupling of two atoms through surface modes for the metal and metamaterial slab. In Sec. IV, the induced entanglement from initial separable state has been calculated. We give a discussion about the influence of dissipation in Sec. V and draw conclusions in Sec. VI.

II. MODEL AND DENSITY MATRIX OF TWO ATOMS

We consider a system of two identical two-level atoms (bold arrows in Fig. 1) separated by a slab with thickness d and indexes ε_M and μ_M, as shown in Fig. 1. The medium where the atoms are located is assumed to be a vacuum for the sake of simplicity. These two identical two-level atoms have a lower level $|g_i\rangle$ and an upper level $|e_i\rangle$ $(i = 1, 2)$ separated by energy $\hbar\omega_0$. We assume that the two atoms are symmetrically located on both sides of the slab at positions $z_1 = z_0$ and $z_2 = d - z_0$ and have the same dipole moment $\mathbf{P} = P\mathbf{e}_x$. The atoms are coupled to the multimode electromagnetic field where all modes are initially in the vacuum $|\{0\}\rangle$. It is convenient to work in the basis of the four Dicke states, defined as [14]

$$\begin{aligned} |4\rangle &= |e\rangle_1|e\rangle_2, \quad |1\rangle = |g\rangle_1|g\rangle_2, \\ |s\rangle &= (|e\rangle_1|g\rangle_2 + |g\rangle_1|e\rangle_2)/\sqrt{2}, \\ |a\rangle &= (|e\rangle_1|g\rangle_2 - |g\rangle_1|e\rangle_2)/\sqrt{2}. \end{aligned} \tag{1}$$

In this basis, the two-atom system behaves as a single four-level system with two unentangled states, the ground state $|1\rangle$ and the upper state $|4\rangle$, and two maximally entangled states, the symmetric state $|s\rangle$ and the antisymmetric state $|a\rangle$. The evolution of the two-atom system is governed by a master equation, which can be solved analytically. The resulting solution is [15]

$$\rho_{44}(t) = \rho_{44}(0)e^{-2\gamma t}, \tag{2}$$

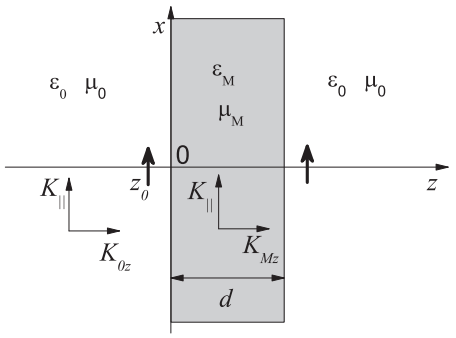

FIG. 1. Scheme of the structure considered. The bold arrows represent two identical atoms.

$$\rho_{ss}(t) = \rho_{ss}(0)e^{-(\gamma+\gamma_{12})t} + \rho_{44}(0)e^{-2\gamma t}\frac{\gamma+\gamma_{12}}{\gamma-\gamma_{12}}[e^{(\gamma-\gamma_{12})t}-1], \tag{3}$$

$$\rho_{aa}(t) = \rho_{aa}(0)e^{-(\gamma-\gamma_{12})t} + \rho_{44}(0)e^{-2\gamma t}\frac{\gamma-\gamma_{12}}{\gamma+\gamma_{12}}[e^{(\gamma+\gamma_{12})t}-1], \tag{4}$$

$$\rho_{sa}(t) = \rho_{sa}(0)e^{-(\gamma+2i\Omega_{12})t} = \rho^*_{as}(t), \tag{5}$$

with $\rho_{11}(t) = 1-\rho_{ss}(t)-\rho_{aa}(t)-\rho_{44}(t)$. In Eqs. (2)–(5), the evolution of the matrix elements depends on three parameters, namely, the decay rate γ, the collective damping rate γ_{12}, and the energy shift Ω_{12}.

For measuring the entanglement between the two atoms, we adopt the concurrence, which is defined by [16]

$$C(t) = \max\{0, C_M(t)\}, \tag{6}$$

where

$$C_M(t) = \sqrt{[\rho_{ss}(t)-\rho_{aa}(t)]^2 - [\rho_{sa}(t)-\rho_{as}(t)]^2} - 2\sqrt{\rho_{11}(t)\rho_{44}(t)}. \tag{7}$$

The quantity $C_M(t)$ is determined by the evolution of the matrix elements, Eqs. (2)–(5), subject to appropriate initial conditions. From Eqs. (2)–(5), we find the following: If $\gamma_{12} = \gamma$, we have $\rho_{44}(t)$ and $\rho_{ss}(t)$ decaying exponentially with rate 2γ, while $\rho_{aa}(t)$ is trapped at $\rho_{aa}(0)$. Consequently, we have $C(t) = \rho_{aa}(0)$. If $\gamma_{12} = -\gamma$, we similarly have $C(t) = \rho_{ss}(0)$. For $\gamma_{12} \approx 0$, all elements except $\rho_{11}(t)$ decay exponentially, and as a result, $C_M(t)$ could be negligible after $t > 1/\gamma$ for an arbitrary initial state. Therefore, constructing a certain environment to get a strong collective damping rate γ_{12} is the key to generating and preserving the entanglement. Thus the control of the collective damping under the structure shown in Fig. 1 is the main objective of this paper.

The expressions for the decay rate γ, the collective damping rate γ_{12}, and the energy shift Ω_{12} for the two atoms are given by [17]

$$\gamma(z_1) = \frac{2}{\hbar\varepsilon_0}\frac{\omega_0^2}{c^2}\mathbf{P}\cdot \mathrm{Im}\overleftrightarrow{\mathbf{G}}(z_1,z_1,\omega_0)\cdot\mathbf{P}, \tag{8}$$

$$\gamma_{21}(z_2,z_1) = \frac{2}{\hbar\varepsilon_0}\frac{\omega_0^2}{c^2}\mathbf{P}\cdot \mathrm{Im}\overleftrightarrow{\mathbf{G}}(z_2,z_1,\omega_0)\cdot\mathbf{P}, \tag{9}$$

$$\Omega_{21}(z_2,z_1) = \frac{1}{\hbar\varepsilon_0}\frac{\omega_0^2}{c^2}\mathbf{P}\cdot \mathrm{Re}\overleftrightarrow{\mathbf{G}}(z_2,z_1,\omega_0)\cdot\mathbf{P}, \tag{10}$$

where the Green's tensors fitted for the structure of Fig. 1 are [18]

$$\overleftrightarrow{G}(z_1,z_1,\omega_0) = \frac{i\mu_0}{2(2\pi)^2}\int d^2\mathbf{K}_{||}\frac{1}{K_z}\sum_{q=e,m}\left[\mathbf{e}_q^+\mathbf{e}_q^+ + e^{-i2K_z z_1}\times\frac{r^q_{ML}+r^q_{RM}e^{2iK_{Mz}d}}{1-r^q_{LM}r^q_{RM}e^{2iK_{Mz}d}}\mathbf{e}_q^-\mathbf{e}_q^+\right],\ z_1\notin[0,d], \tag{11}$$

$$\overleftrightarrow{G}(z_2,z_1,\omega_0) = \frac{i\mu_0}{2(2\pi)^2}\int d^2\mathbf{K}_{||}\frac{1}{K_z}e^{iK_z(z_2-d-z_1)}\times\sum_{q=TE,TM}\frac{t^q_{ML}t^q_{RM}e^{iK_{Mz}d}}{1-r^q_{LM}r^q_{RM}e^{2iK_{Mz}d}}\mathbf{e}_q^+\mathbf{e}_q^+, \tag{12}$$

Here $K_z = \sqrt{\varepsilon_0\mu_0\omega^2/c^2 - K_{||}^2}$ and $K_{Mz} = \sqrt{\varepsilon_M\mu_M\omega^2/c^2 - K_{||}^2}$ are the z components of the wave vector in vacuum and in the slab, respectively, while $K_{||}$ is the component parallel to the interface. The reflective coefficients for TE and TM polarization modes incident from the slab (M) to the left (L) or right (R) are

$$r^{TE}_{LM} = r^{TE}_{RM} = \frac{\mu_0 K_{Mz}-\mu_M K_{0z}}{\mu_0 K_{Mz}+\mu_M K_{0z}},$$
$$r^{TM}_{LM} = r^{TM}_{RM} = \frac{\varepsilon_0 K_{Mz}-\varepsilon_M K_{0z}}{\varepsilon_0 K_{Mz}+\varepsilon_M K_{0z}}. \tag{13}$$

Similar expressions can be given for the transmission coefficients t^q_{ML} and t^q_{RM}. Note $\mathbf{e}_q^+$ ($\mathbf{e}_q^-$) is the unit vector of electric field incident from left (right) to right (left) for q polarization in the vacuum, which is

$$\mathbf{e}^{\pm}_{TM}(\mathbf{K}_{||}) = \frac{1}{K_0}\left(\mp K_{0z}\frac{\mathbf{K}_{||}}{K_{||}} + K_{||}\mathbf{e}_z\right),\quad \mathbf{e}^{\pm}_{TE}(\mathbf{K}_{||}) = \frac{\mathbf{K}_{||}}{K_{||}}\times\mathbf{e}_z. \tag{14}$$

The two atoms have the same decay rate γ due to their symmetric location.

The integrations in Eqs. (11) and (12) are taken over all electromagnetic modes, which include propagating wave modes, waveguide modes, and surface modes [19]. When atoms are far away from the slab, the contribution of the waveguide modes and the surface modes can be neglected due to the exponential decrease of their amplitudes. However, when the atoms are close to the slab, the surface modes dominate the decay rate and the collective damping rate due to high mode density.

In the next section, we analyze the role of the surface modes played in the collective damping rate and would like to find a way to control the collective damping rate in the structure of Fig. 1.

III. THE DEPENDENCE OF THE COLLECTIVE DAMPING RATE ON THE SURFACE MODES

The surface modes in a metal have been studied extensively, and their properties are discussed in detail in [20]. The surface mode is referred to as the surface plasmon polariton (SPP) mode. These modes play a key role in the control of molecular fluorescence and phosphorescence [21–24] as

TABLE I. Analysis of the terms in Eqs. (15) and (16).

Function	$K_{\|\|} = \omega/c$	$K_{\|\|} = \infty$	Property
k_M/k_0	∞	1	monotonously decreasing
$\coth(k_M d/2)$	$\coth[\sqrt{\omega^2/c^2(\|\varepsilon_M\|+1)}d/2]>1$	1	monotonously decreasing
$\tanh(k_M d/2)$	$\tanh[\sqrt{\omega^2/c^2(\|\varepsilon_M\|+1)}d/2]<1$	1	monotonously increasing

well as the modification of the decay rate of an atom or a quantum dot [25–27]. However, most of these works are focused on a single-body system. Recently, the effect of the surface mode on a multibody system has attracted a lot of attention [12,13,28,29]. For the structure as shown in Fig. 1, the surface modes exist only when $1 - r^q_{LM} r^q_{RM} e^{2iK_{Mz}d} = 0$, which corresponds to the pole of the Green's tensors of Eqs. (11) and (12) [19]. To satisfy this condition, the necessary condition is that either the permittivity or permeability is negative.

In addition to metals, metamaterials also support surface modes [30,31]. Metamaterials are a new kind of man-made material in which the effective permittivity or the effective permeability or both are negative [32]. They provide a new way to manipulate the electromagnetic properties of materials at will. The material with negative effective permittivity [33] is equivalent to metal. The material with negative effective permeability [34] is referred to as negative-permeability materials and has similar properties to metals. The materials with both negative effective permittivity and permeability are the so-called left-handed materials (LHM) [35,36]. In a left-handed material, the electric field, the magnetic field, and the wave vector form the left-handed triplet. In this section, we analyze the properties of the surface modes in a slab with different indexes and their influence on the collective damping. We divide our analysis into two parts. The first part focuses on the case $\varepsilon_M < 0$ and $\mu_M = 1$, and the other refers to the case of $\varepsilon_M < 0$ and $\mu_M < 0$.

A. Slab with $\varepsilon_M < 0$ and $\mu_M = 1$

In this case, the refractive index of the slab is imaginary, and there is only evanescent electromagnetic field inside the slab. Metals belong to this case, and it is well known that metals are opaque to propagating electromagnetic waves. The two atoms separated by a metal slab could not be coupled through the propagating wave. As the surface mode is local near the interface of the slab, intuition leads us to believe that it would result in strong collective damping between the two atoms near the metal. However, the situation is different.

The range of $K_{\|}$ for the surface modes in this case should be larger than ω/c in order to get pure imaginary z components of wave vectors in all spaces, i.e., $K_z = ik_0$ and $K_{Mz} = ik_M$. There are only TM polarized surface modes with dispersion relations

$$\varepsilon_M(\omega) = -\frac{k_M}{k_0}\coth(k_M d/2), \tag{15}$$

$$\varepsilon_M(\omega) = -\frac{k_M}{k_0}\tanh(k_M d/2). \tag{16}$$

The mode defined in Eq. (15) is symmetric, while that defined in Eq. (16) is antisymmetric.

According to Table I, when $K_{||}$ varies from ω/c to infinity, the right sides of both Eqs. (15) and (16) change from -∞ to -1. Therefore, for a usual metal with$\varepsilon_M < -1$, there must be solutions for both Eqs. (15) and (16). As a result, a usual metal slab with$\varepsilon_M < -1$ supports both symmetric and antisymmetric surface modes independent of the thickness.

As an example, we consider a Ag film with $\omega_0 = 4.3 \times 10^{15}$ Hz whose permittivity at the operating wavelength $\lambda = 440$ nm is equal to $\varepsilon_M = -6.0$. Here we ignore the imaginary part of the permittivity [37]. In Fig. 2(a), we plot the dispersion relation of the surface modes as a function of the slab thickness. It is clear that there are

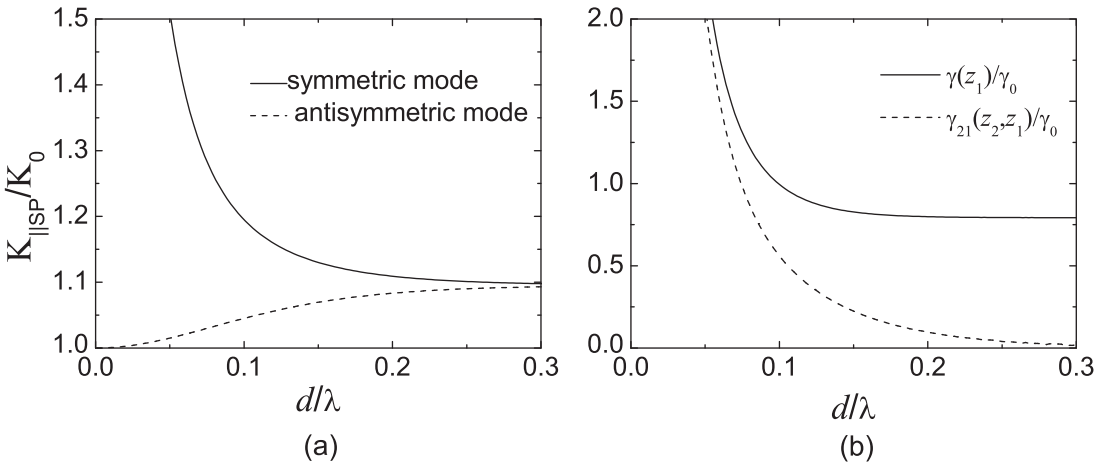

FIG. 2. (a) Dispersion relations of surface modes vs thickness d and (b) the decay rate of atom 1 $\gamma(z_1,z_1)$ and the collective damping rate $\gamma_{21}(z_2,z_1)$ vs d with $\varepsilon_M = -6$, atom 1 at $z_1 = -0.05\lambda$, and atom 2 at $z_2 = d - z_1$.

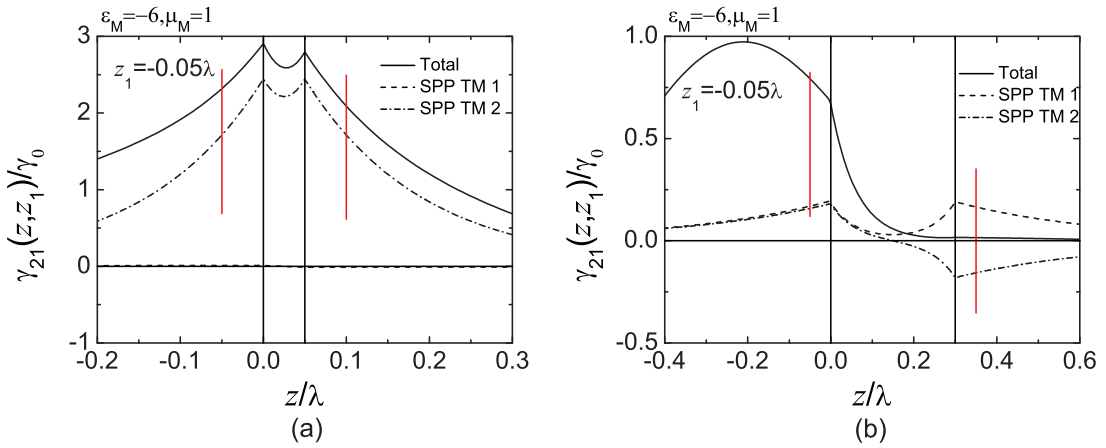

FIG. 3. (Color online) The normalized $\gamma_{21}(z,z_1)$ vs z for (a) $d = 0.05\lambda$ and (b) $d = 0.3\lambda$. The two red solid lines indicate the positions of the two atoms ($z_2 = d - z_1$) shown in Fig. 1.

two modes for any thickness. However, for small thickness $d < 0.2\lambda$, the propagation constants ($K_{\|SP}$) of these two modes can be distinguished, whereas they become degenerate for larger thickness ($d > 0.2\lambda$). Then with atom 1 located at $z_1 = -0.05\lambda$ and atom 2 located at $z_2 = d - z_1$, we can compare the decay rate $\gamma(z_1,z_1)$ with the collective damping $\gamma_{21}(z_2,z_1)$ for different d in Fig. 2(b). It is shown that the collective damping can be ignored in comparison with the decay rate for $d > 0.2\lambda$. Only for $d < 0.06\lambda$ does the collective damping rate approach the decay rate.

To make clear the role of the surface modes in the collective damping, we plot the field emitted by atom 1 as a function of position z. According to the electromagnetic theory [38], the field at position z emitted by atom 1 located at z_1 can be expressed with a Green's tensor as

$$\mathbf{E}(z,z_1) = \frac{\omega_0^2}{c^2}\overleftrightarrow{G}(z,z_1,\omega_0)\cdot\mathbf{P}. \tag{17}$$

What we are interested in is the x component of the emitted field as only this component can act on atom 2 with polarization $\mathbf{P} = P\mathbf{e}_x$. The x component, by using Eq. (9), is

$$E_x(z,z_1) = \frac{\omega_0^2}{c^2}\mathbf{e}_x\cdot\overleftrightarrow{G}(z,z_1,\omega_0)\cdot\mathbf{P} = \frac{\hbar\varepsilon_0}{2P}\gamma_{21}(z,z_1). \tag{18}$$

It is clear from Eq. (18) that, apart from a constant $\hbar\varepsilon_0/2P$, the x component of the field emitted by atom 1 is determined by $\gamma_{12}(z,z_1)$. Thus $\gamma_{12}(z,z_1)$ yields the field distribution, whereas $\gamma_{12}(z_2,z_1)$ is the collective damping rate.

In Fig. 3, by setting $z_1 = -0.05\lambda$ and $\varepsilon_M = -6$, we plot $\gamma_{21}(z,z_1)$ versus z for $d = 0.05\lambda$ and for $d = 0.3\lambda$. Two dashed curves in Fig. 3 are the contribution of the two surface fields emitted by atom 1, one with a symmetric profile and the other with an antisymmetric profile. On the right side of the slab ($z > d$), these two fields are opposite. For $d = 0.05\lambda$, the amplitudes of the symmetric and the antisymmetric modes are quite different due to different propagation constant $K_{\|SP}$, and the antisymmetric modes can be ignored. Only the symmetric mode contributes to the emitted field, and the field on the right is nearly equal to that on the left. However, for $d = 0.3\lambda$, the two modes have nearly the same amplitudes, and the total field on the right side is nearly zero, leading to a negligible propagation field.

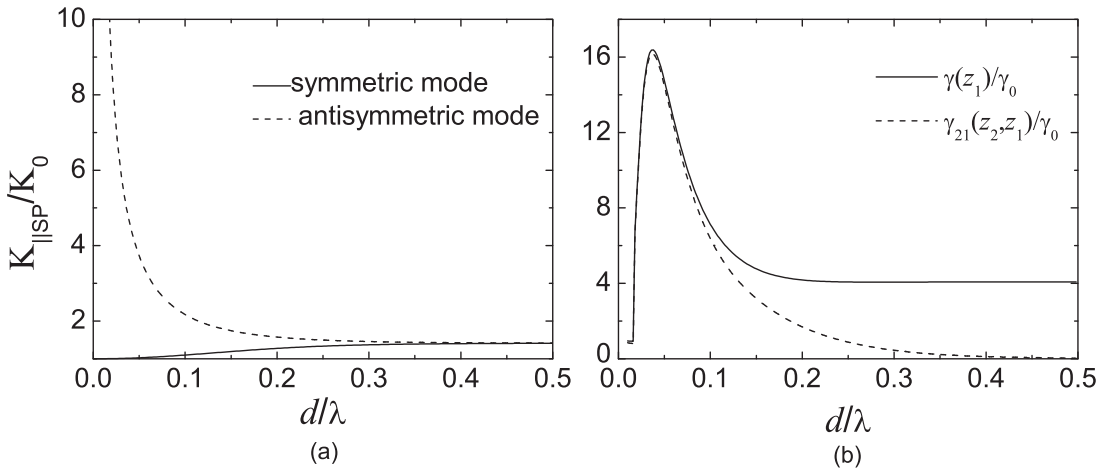

FIG. 4. (a) Dispersion relations of surface modes vs thickness d and (b) the decay rate of atom 1 $\gamma(z_1,z_1)$ and the collective damping rate $\gamma_{21}(z_2,z_1)$ vs d with $\varepsilon_M = -2$, where atom 1 is at $z_1 = -0.05\lambda$ and atom 2 is at $z_2 = d - z_1$.

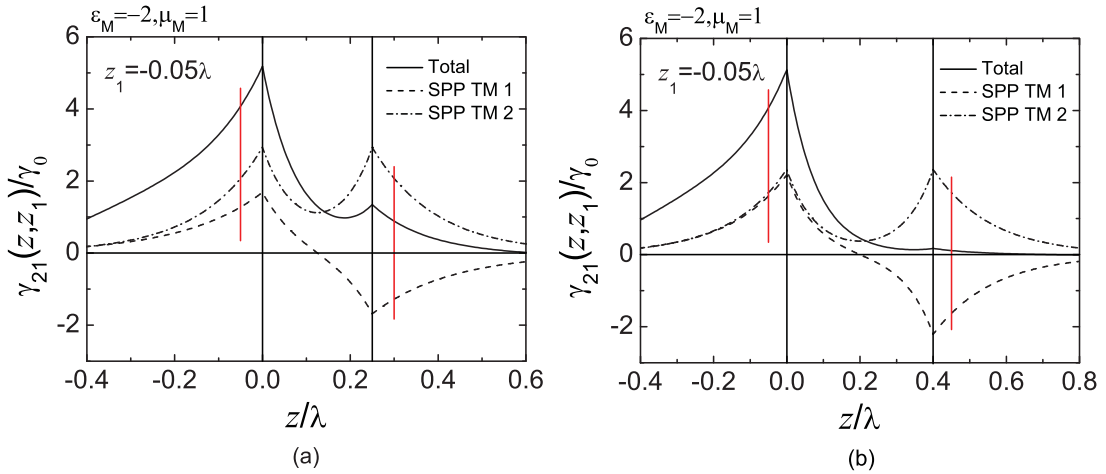

FIG. 5. (Color online) The normalized $\gamma_{21}(z,z_1)$ vs z with (a) $d = 0.25\lambda$ and (b) $d = 0.4\lambda$. The two red solid lines indicate the positions of the two atoms ($z_2 = d - z_1$) shown in Fig. 1.

We note that $\gamma_{21}(z = z_1,z_1)$ is just the decay rate of atom 1 at z_1, while $\gamma_{21}(z = z_2,z_1)$ is the collective damping between the two atoms. These are marked by the intersection between the black curves and the short red lines in Fig. 3. This makes clear the interpretation of Fig. 2(b). The collective damping should be significant only for a thin metal slab, which is consistent with the result in Ref. [28]. In addition, with higher $|\varepsilon_M|$, a significant collective damping is obtained in a thin slab, and the contribution of the surface mode becomes lower. So for a usual metal film such as Ag and Au as well as Cu, with permittivity smaller than -100 for $\lambda > 1\ \mu$m [37], the surface mode can be neglected for an atom near usual metals.

However, when $|\varepsilon_M|$ tends to 1, the contribution of the surface mode becomes dominant for arbitrary thickness. For example, we set $\varepsilon_M = -2$ and $\mu_M = 1$ and repeat the results of Figs. 2 and 3 in Figs. 4 and 5. From Figs. 4 and 5, it is clear that the superposition of surface modes determines the collective damping. For a thin slab, the symmetric surface mode dominates the collective damping, and then apparent collective damping appears. However, for a thicker slab, the symmetric and the antisymmetric surface modes have the same contributions to the collective damping, thus resulting in negligible collective damping.

Besides a thin metal slab, there is another way to get considerable collective damping, which is cancelling one of these two kinds of surface modes. According to Table I, the only possible way is to choose $\varepsilon_M \in (-1,0)$, in which only antisymmetry surface modes would survive if the smallest value of function $\tanh(k_M d)k_M/k_0$ is less than $|\varepsilon_M|$. Such parameters can be realized by metamaterials. In Fig. 6(a), we mark the parameter region of ε_M as well as thickness d supporting two antisymmetric modes with shading. As an example, we choose the slab with ($\varepsilon_M = -0.75, d = 0.1\lambda$), and locate atom 1 at $z_1 = -0.2\lambda$, then plot $\gamma_{21}(z,z_1)$ as a function of z in Fig. 6(b). It is shown that the two surface modes are both antisymmetric, and their constructive superposition leads to nearly the same amplitude distribution on both sides of the slab. As the two atoms are symmetrically located on both sides of the slab (marked by short red lines), the collective

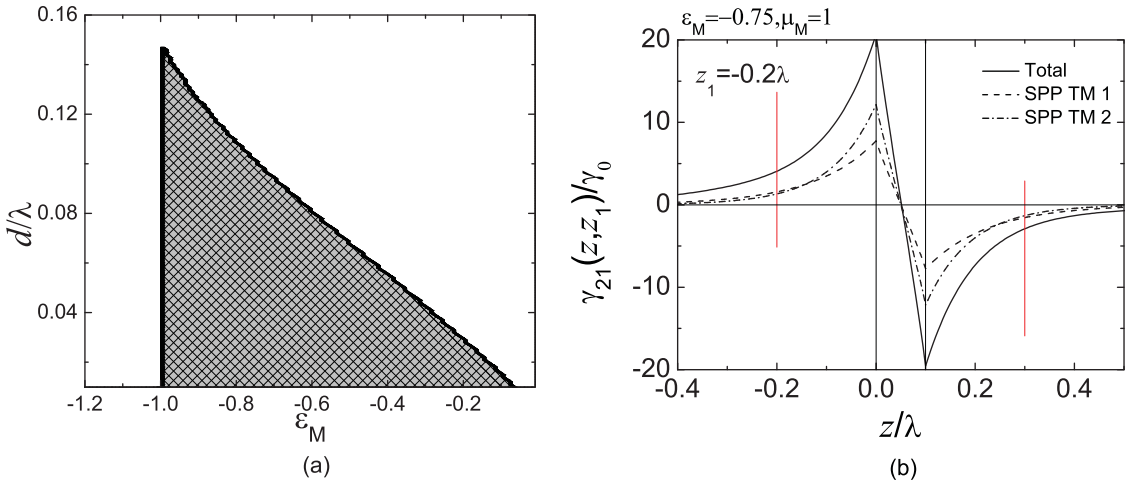

FIG. 6. (Color online) (a) Parameter region of ε_M and d supporting two antisymmetry surface modes. (b) Normalized $\gamma_{21}(z,z_1)$ vs z on the slab with $\varepsilon_M = -0.75$ and $d = 0.1\lambda$, while atom 1 is located at $z_1 = -0.2\lambda$ and atom 2 is located at $z_2 = d - z_1$.

TABLE II. Analysis of the terms in dispersion relations for LHM with $n_M \leqslant -1$.

Function	$K_{\|\|} = \|n_M\|\omega/c$	$K_{\|\|} = \infty$	Property
k_M/k_0	0	1	monotonously increasing
$\coth(k_M d/2)$	∞	1	monotonously decreasing
$\tanh(k_M d/2)$	0	1	monotonously increasing
$\coth(k_M d/2)k_M/k_0$	$2(\sqrt{n_M^2-1}\omega d/c)^{-1}$	1	not sure
$\tanh(k_M d/2)k_M/k_0$	0	1	monotonously increasing

damping is almost equal to the decay rate. The tiny difference between them originates from the asymmetric radiative field.

B. LHM slab with $\varepsilon_M < 0$ and $\mu_M < 0$

LHM are man-made materials with $\varepsilon_M < 0$ and $\mu_M < 0$. The wave vector of the electromagnetic field in LHMs is opposite to the energy flux, which makes the LHM act as phase compensation device, such as a perfect lens [39] and a broadband ground-plane cloak [40]. In Ref. [41], it was shown that two atoms separated by an ideal LHM ($\varepsilon_M = \mu_M = -1$) slab have strong collective damping and lead to superradiance without the consideration of surface modes. However, this result is only good for the ideal case $\varepsilon_M = \mu_M = -1$. Here we consider more general LHM indexes, in which the collective damping through propagating modes is weak due to reflection and invalidates the phase compensation. To deal with this problem, we resort to manipulating surface modes of LHM to control the collective damping.

As opposed to a metal that can only support TM surface modes, the LHM slab can support both TE and TM surface modes due to $\varepsilon_M < 0$ and $\mu_M < 0$. According to Ref. [31], besides the TM modes of Eqs. (15) and (16), dispersion relations for TE surface modes are as follows:

$$\mu_M(\omega) = -\frac{k_M}{k_0}\tanh(k_M d/2), \tag{19}$$

$$\mu_M(\omega) = -\frac{k_M}{k_0}\coth(k_M d/2). \tag{20}$$

The mode defined in Eq. (19) is symmetric, while that defined in Eq. (20) is antisymmetric. It follows, on combining Eqs. (19) and (20) with Eqs. (15) and (16), that there are four dispersion relations for LHM. Since the ranges of permittivity and permeability of LHM are much wider than metal, we only focus on the case $n_M = \sqrt{\varepsilon_M}\sqrt{\mu_M} \leqslant -1$. In this case, the range of $K_{\|}$ corresponding to surface modes is $K_{\|} \in (|n_M|\omega/c,\infty)$, which is different from that of metal with $K_{\|} \in (\omega/c,\infty)$. Therefore, here k_M/k_0 is a monotonously increasing function from 0 to 1 with $K_{\|}$. The analysis of terms in Eqs. (15), (16), (19), and (20) for $n_M \leqslant -1$ are presented in Table II.

In order to clarify the discussion for LHM with $|n_M| > 1$, we consider two subcases, (i) $|\varepsilon_M|, |\mu_M| \geqslant 1$ and (ii) $\varepsilon_M < -1$, $\mu_M > -1$.

1. ε_M and $\mu_M \leqslant -1$

With Table II in mind, it is easy to see that Eqs. (16) and (19) have no solution when ε_M and $\mu_M \leqslant -1$. In other words, only the TE antisymmetric mode Eq. (20) and TM symmetric mode Eq. (15) may exist. However, their coexistence can lead to a destructive superposition for the collective damping. To deal with this problem, a feasible way is to suppress one mode and enhance the other. We give the conditions for different solutions in Table III.

According to Table III, we classify surface modes corresponding to ε_M and μ_M for fixed thickness $d = 0.2\lambda$ in Fig. 7(a). The indexes of (ε_M, μ_M) falling in the yellow region can support both the TM symmetric surface mode and the TE antisymmetric surface mode, while (ε_M, μ_M) falling in the green (blue) region can support only the TE antisymmetric (TM symmetric) surface modes. For example, we choose the parameters ($\varepsilon_M = -3$, $\mu_M = -1$) corresponding to only the TE antisymmetric surface mode and plot the field distribution emitted by atom 1 in Fig. 7(b). As expected, the collective damping $\gamma_{21}(z = z_2, z_1)$ (intersection between the right short red line and the solid curve) has nearly the same amplitude as the decay rate $\gamma_{21}(z = z_1, z_1)$ (with the left short red line). Conversely, we pick up the parameters ($\varepsilon_M = -1.5$, $\mu_M = -1.2$) corresponding to both antisymmetric and symmetric surface modes and plot the field distribution along the z axis in Fig. 7(c). Due to the destructive superposition, the field on the right side of the slab is much smaller than that on the left side. More importantly, the collective damping $\gamma_{21}(z = z_2, z_1)$ in this case is nearly zero. Therefore, though the LHM slab is transparent to an

TABLE III. The conditions for different solutions under ε_M and $\mu_M \leqslant -1$.

Solution	Condition
TM symmetric surface mode only	$\|\varepsilon_M\| < 2(\sqrt{n_M^2-1}\omega d/c)^{-1} < \|\mu_M\|$
TE antisymmetric surface mode only	$\|\mu_M\| < 2(\sqrt{n_M^2-1}\omega d/c)^{-1} < \|\varepsilon_M\|$
Both TE and TM surface modes	$\|\varepsilon_M\|, \|\mu_M\| < 2(\sqrt{n_M^2-1}\omega d/c)^{-1}\|$
No surface mode	other

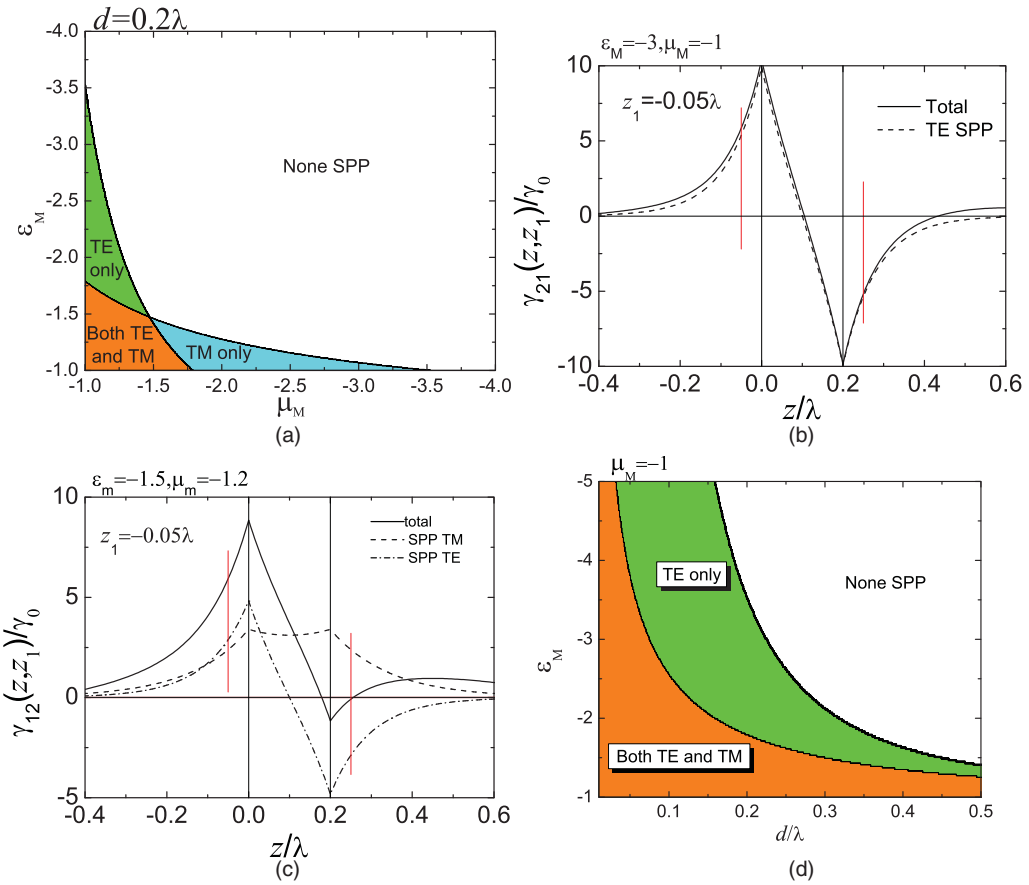

FIG. 7. (Color online) The classification of surface modes according to Table III for (a) fixed thickness $d = 0.2\lambda$ and (d) fixed $\mu_M = -1$. The normalized $\gamma_{21}(z,z_1)$ vs z with $z_1 = -0.05\lambda$ and $d = 0.2\lambda$ for (b) $\varepsilon_M = -3$, $\mu_M = -1$ and (c) $\varepsilon_M = -1.5$, $\mu_M = -1.2$. Notice $z_2 = d - z_1$.

electromagnetic wave, two atoms separated by it could be decoupled by manipulating the surface modes. We can judge the property of the surface modes for an arbitrary LHM slab according to Table III even when we fix $\mu_M = -1$, as shown in Fig. 7(d).

2. $\varepsilon_M < -1$ and $\mu_M > -1$

Similar to the discussion in Sec. III B 1, we now consider the case of $\varepsilon_M < -1$ and $\mu_M > -1$. With the help of Table II, it is clear that there must be one solution for Eq. (19) and no solution for Eq. (16). The right sides of Eqs. (15) and (20) change from $2(\sqrt{n_M^2 - 1}\omega d/c)^{-1}$to 1 with $K_{||}$. We compare the properties of the surface modes in Table IV. It is shown that, if $2(\sqrt{n_M^2 - 1}\omega d/c)^{-1} > |\mu_M|$, there are only symmetric modes. Otherwise, the symmetric and the antisymmetric modes coexist for $2(\sqrt{n_M^2 - 1}\omega d/c)^{-1} < |\mu_M|$.

In Fig. 8(a), we plot $2(\sqrt{n_M^2 - 1}\omega d/c)^{-1}$as a function of d with fixed ($\varepsilon_M = -1.5$, $\mu_M = -0.9$). According to Table IV, there are three regions of d possessing different kinds of surface modes, i.e., both TE and TM symmetry modes for $d < 0.36\lambda$, only the TE symmetry mode for $0.36\lambda < d < 0.6\lambda$, and TE symmetric and antisymmetric modes for $d > 0.36\lambda$. As an example, we choose $d = 0.2\lambda, 0.5\lambda$,and λ and then plot the corresponding field distributions in Figs. 8(b), 8(c), and 8(d), respectively.

In Figs. 8(b) and 8(c), the collective damping $\gamma_{21}(z = z_2, z_1)$ is significant only due to the symmetry mode. However, the density of state of the surface modes decreases with an increase of thickness. The collective damping

TABLE IV. Conditions for different solutions under $\varepsilon_M < -1$ and $\mu_M > -1$.

Condition	TM symmetric (14)	TM antisymmetric (15)	TE symmetric (16)	TE antisymmetric (17)
$2(\sqrt{n_M^2 - 1}\omega d/c)^{-1} > \lvert\varepsilon_M\rvert$	yes	no	yes	no
$\lvert\varepsilon_M\rvert > 2(\sqrt{n_M^2 - 1}\omega d/c)^{-1} > \lvert\mu_M\rvert$	no	no	yes	no
$\lvert\mu_M\rvert > 2(\sqrt{n_M^2 - 1}\omega d/c)^{-1}$	no	no	yes	yes

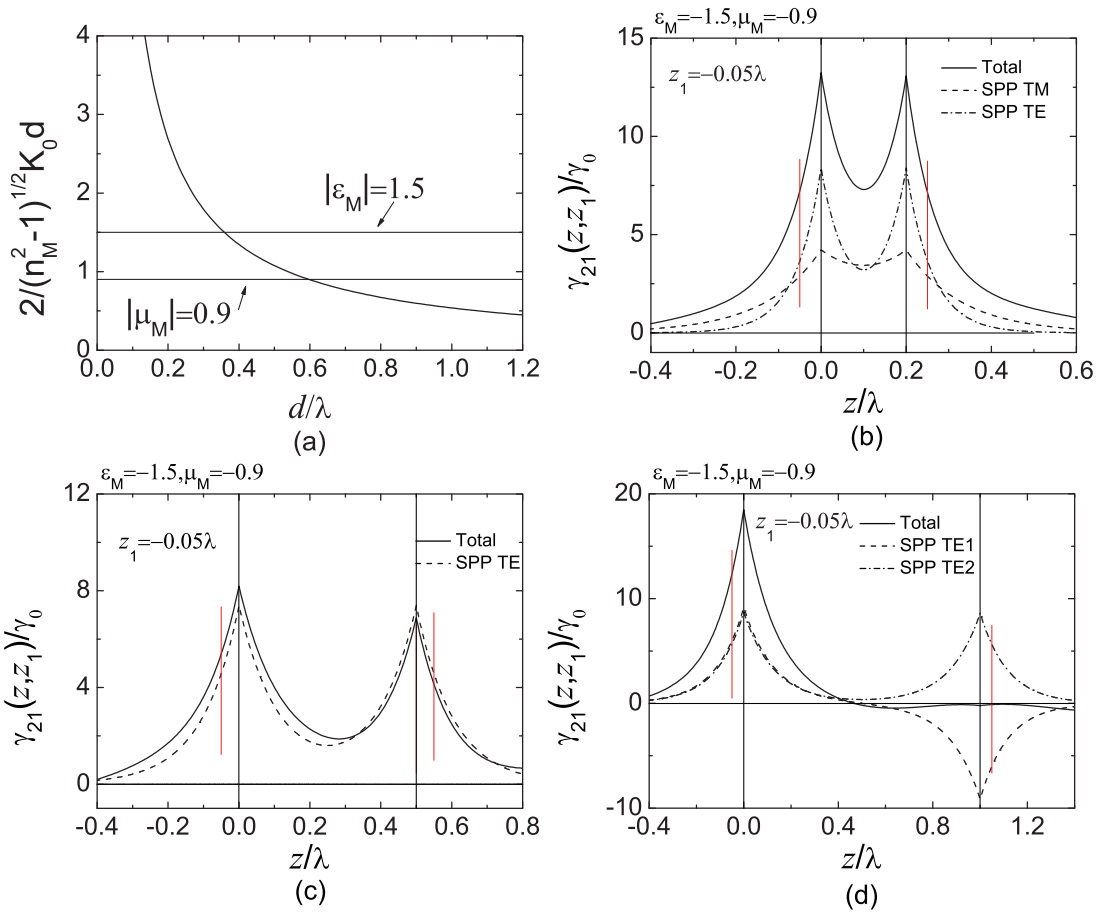

FIG. 8. (Color online) (a) For a slab with $\varepsilon_M = -1.5$ and $\mu_M = -0.9$, classification of the surface modes according to Table IV with d. Normalized $\gamma_{21}(z,z_1)$ with z for (b) $d = 0.2\lambda$, (c) $d = 0.5\lambda$, and (d) $d = \lambda$. Here $z_2 = d - z_1$.

$\gamma_{21}(z = z_2,z_1)$ is therefore smaller than the decay rate $\gamma(z_1) = \gamma_{21}(z = z_1,z_1)$ due to the relative apparent radiative decay rate, as shown in Fig. 8(c). When $d = \lambda$, the destructive superposition of symmetric and antisymmetric surface modes nearly cancels the collective damping $\gamma_{21}(z = z_2,z_1)$, as shown in Fig. 8(d).

In conclusion, the choice of the appropriate parameters can enhance or inhibit the collective damping relative to the decay rate based on the properties of the surface modes. This is useful in controlling the entanglement, as we discuss in the following section.

IV. GENERATION OF ENTANGLEMENT FROM AN INITIAL SEPARABLE STATE

We consider that, initially, atom 1 is in the excited state, while atom 2 is in the ground state, i.e.,

$$\psi(0) = |e\rangle_1 |g\rangle_2 |0\rangle . \tag{21}$$

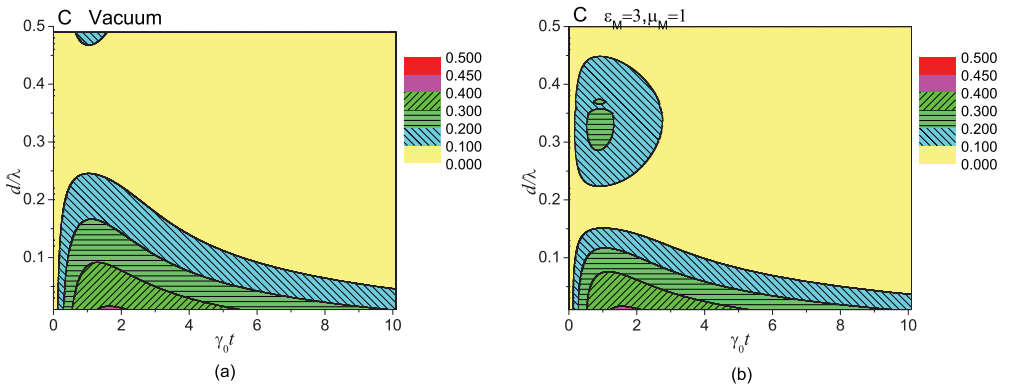

FIG. 9. (Color online) Concurrence evolution vs thickness for (a) the vacuum and (b) the dielectric slab with $\varepsilon_M = 3$ and $\mu_M = 1$. Atom 1 is at $z_1 = -0.05\lambda$, while atom 2 is at $z_2 = d - z_1$.

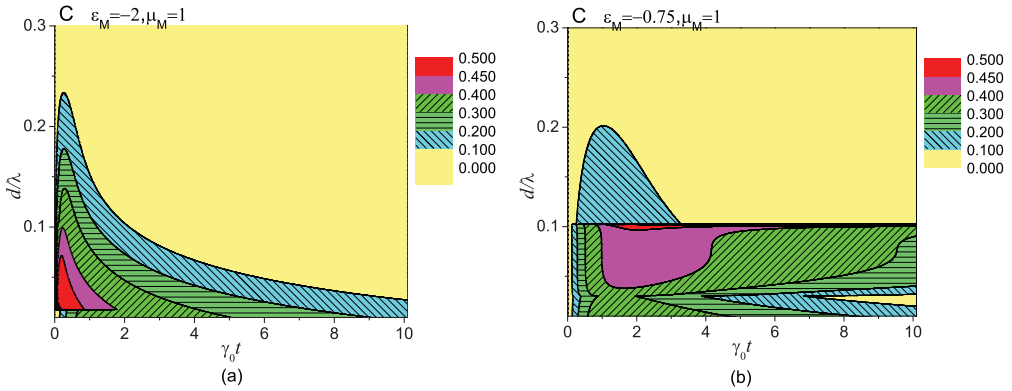

FIG. 10. (Color online) Concurrence evolution with time for different thicknesses for (a) a metal with $\varepsilon_M = -2$ and $\mu_M = 1$ and (b) a slab with $\varepsilon_M = -0.75$ and $\mu_M = 1$. $z_1 = -0.05\lambda$, $z_2 = d - z_1$.

In this case, the initial values of density matrix elements are

$$\rho_{ss}(0) = \rho_{sa}(0) = \rho_{as}(0) = \rho_{aa}(0) = \tfrac{1}{2},$$
$$\rho_{44}(0) = \rho_{11}(0) = 0. \tag{22}$$

It follows, on inserting Eq. (22) into Eqs. (2)–(7), that the concurrence is given by

$$C(t) = \max\{0, \sqrt{0.25[e^{-(\gamma+\gamma_{12})t} - e^{-(\gamma-\gamma_{12})t}]^2 + \sin(2\Omega_{12}t)e^{-2\gamma t}}\}. \tag{23}$$

An inspection of Eq. (23) shows that, at initial time, two atoms are disentangled with $C(0) = 0$. If the collective damping rate γ_{12} is present, the entanglement may appear with time. To test the relation between collective damping rate and the entanglement, we place atom 1 at $z_1 = -0.05\lambda$ and the atom 2 at $z_2 = d - z_1$ and then vary the parameter of the slab to get the evolution of concurrence.

In Fig. 9, we plot the concurrence versus the slab thickness with atom 1 at $z_1 = -0.05\lambda$ and atom 2 at $z_2 = d - z_1$ for the vacuum and a dielectric slab. It is shown that the maximum concurrence can reach to 0.4 only for a thin thickness, $d > 0.02\lambda$. This, however, is hard to achieve experimentally. When the thickness is larger than 0.02λ, the maximum concurrence decreases quickly with the thickness and is no more than 0.3 for $d > 0.1\lambda$. As only the propagation field contributes to the collective damping in two cases, the collective damping decreases continuously with an increase of thickness, so does the concurrence.

We also check the case of the slab with $\varepsilon_M = -2 < 0$ and $\mu_M = 1$ and plot the concurrence evolution versus the slab thickness with atom 1 at $z_1 = -0.05\lambda$ and atom 2 at $z_2 = d - z_1$in Fig. 10(a). For this slab, the maximum concurrence decreases monotonically with the thickness for $d > 0.04\lambda$. This is consistent with Fig. 4(a) (collective damping versus the thickness). On comparing Fig. 10(a) with Fig. 4(a), we find that the collective damping determines the concurrence: an increase of the thickness results in a decrease of the collective damping, which leads to a decrease in concurrence. However, for $\varepsilon_M = -0.75$, due to the existence of two antisymmetric modes for $d < 0.1\lambda$ with no surface mode for $d > 0.1\lambda$, as shown in Fig. 6(a), the two atoms separated by such a slab will induce a large concurrence for $d < 0.1$ and a small concurrence for $d > 0.1\lambda$, as shown in Fig. 10(b). We thus note the threshold effect of the concurrence around $d = 0.1\lambda$, which may be a potential quantum switch of entanglement.

Finally, we check the cases of the LHM slab. Corresponding to Fig. 7(a), we plot the concurrence evolution versus permittivity with fixed $\mu_M = -1.2$ and $d = 0.2\lambda$ in Fig. 11(a). Although there is no surface mode for $|\varepsilon_M| > 2.4$,

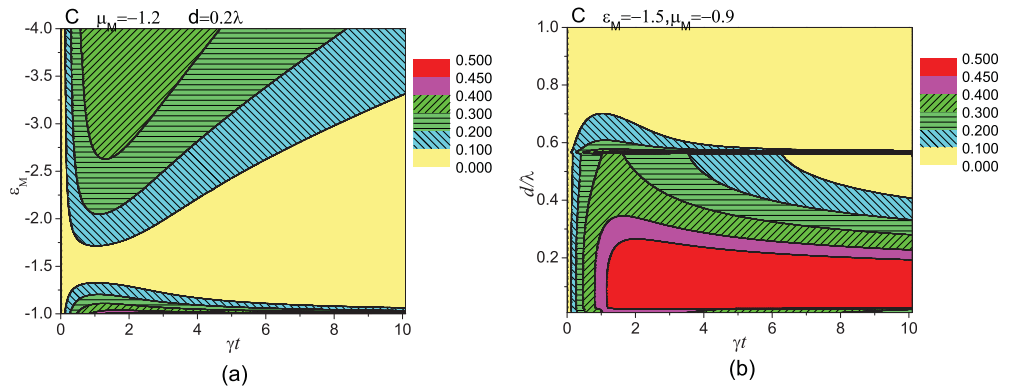

FIG. 11. (Color online) (a) Concurrence evolution vs ε_M with $\mu_M = -1.2$ and $d = 0.2\lambda$. (b) Concurrence evolution vs thickness with $\varepsilon_M = -2$ and $\mu_M = -0.9$. Atom 1 is at $z_1 = -0.05\lambda$, while atom 2 is at $z_2 = d - z_1$.

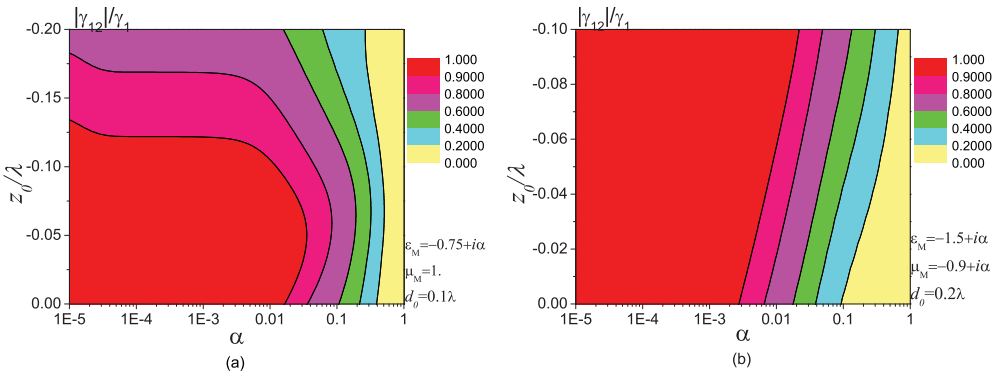

FIG. 12. (Color online) The quantity $|\gamma_{12}(z_1,z_2)|/\gamma_1(z_1)$ as a function of z_0 and dissipation α. $z_1 = z_0$, $z_2 = d_0 - z_0$; other indexes are shown on the plots.

entanglement can also be generated due to the focus effect of the LHM on the propagation field. It is interesting to note the following. When $\varepsilon_M \approx -1.5$, no entanglement can be generated, accompanied by negligible collective damping due to the destructive superposition of the surface modes. Therefore, we can use LHM so that there is no interaction between two closely located atoms (i.e., they are insulated from each other). On the other hand, corresponding to Fig. 8(a), we plot the concurrence evolution versus the thickness with fixed $\varepsilon_M = -2$ and $\mu_M = -0.9$ in Fig. 11(b). It is shown that the maximum concurrence for $d < 0.59\lambda$ is much larger than that for $d > 0.59\lambda$. This effect can be explained by the character of the collective damping as shown in Fig. 8(a): the collective damping is large for $d < 0.59\lambda$ due only to the symmetric surface mode, while the collective damping is negligible for $d > 0.59\lambda$ due to the coexistence of both the symmetric and the antisymmetric surface modes. So, in this case, surface modes play the key role in providing large collective damping and inducing the entanglement from the initial separable state.

Here we just take the initial state with $\psi(0) = |e\rangle_1|g\rangle_2|0\rangle$ into account to show the effect of collective damping on entanglement. However, it has been shown [8,11–13] that a large collective damping can prolong entanglement for an initial entangled state and induce entanglement for an initial separated state, while the opposite situation happens for negligible collective damping.

V. THE INFLUENCE OF DISSIPATION

A real metamaterial is always accompanied with dissipation, which is characterized by the small imaginary parts of the indexes ε_M and μ_M. The influence of the dissipation must therefore be taken into account. With dissipation, there is another decay channel for an atom near the slab, namely, the decay through dissipation [19]. Such decay has no contribution to the collective damping because the energy in this decay process will be transformed into heat in the slab. The dissipation can therefore increase the difference between the decay rate and the collective damping rate and weaken the generation and preservation of entanglement. Here we define the quantity $|\gamma_{12}(z_1,z_2)|/\gamma_1(z_1)$ as relative collective damping. Complete collective damping happens only if $|\gamma_{12}(z_1,z_2)|/\gamma_1(z_1)$ tends to 1. We choose the cases in Figs. 6(b) and 8(b) to check the influence of dissipation as these cases correspond to complete collective damping for a transparent slab. Now considering the dissipation, we plot $|\gamma_{12}(z_1,z_2)|/\gamma_1(z_1)$ as a function of the dissipation coefficient α and the atomic position z_0 in Fig. 12. We note that the two atoms are always located symmetrically all the time, i.e., at $z_1 = z_0$ and at $z_2 = d_0 - z_0$. It is clear that, when $\alpha \to 1$, the quantity $|\gamma_{12}(z_1,z_2)|/\gamma_1(z_1)$ tends to zero. However, $|\gamma_{12}(z_1,z_2)|/\gamma_1(z_1)$ is larger than 0.9 even if $\alpha > 0.01$ for appropriate locations of atoms. Recently, the maximum figures of merit [Im(n)/Re(n)] in experiment reach 8 at $\lambda = 2.4\ \mu$m for 3D negative index metamaterials formed by nanotransfer printing [42], and the theoretic predicted maximum FOM is 15.2 at 408 nm by optimizing the fishnet structure metamaterial [43]. Therefore $\alpha \sim 0.01$ may be realizable in the not-so-distant future.

VI. CONCLUSION

We believe that, with the developments in the fields of quantum information and quantum computation, there will soon be great interest and effort in integrating and miniaturizing quantum devices. At the heart of any potential quantum device lies the creation and control of entanglement between qubits. For a solid-state device, the qubits would be atoms, and a possible method would be to use the present integration chip (IC) techniques.

In this paper, we have discussed, with an eye for potential quantum devices, the collective damping between the two atoms separated by a slab. This is the simplest model for localizing and separating qubits spatially at a subwavelength scale. Specifically, we focus on the effect of surface modes on collective damping between two such atoms as the surface mode is local near the surface of the slab. It is known that there are two kinds of surface modes in a slab, symmetric and antisymmetric. Choosing the appropriate index of the slab can keep down only one kind of mode, so that the two atoms can have significant collective damping through the surface mode. On the other hand, choosing indexes to retain both symmetric and antisymmetric modes can lead to negligible collective damping. We analyzed the index region (including permittivity, permeability, and thickness) of the slab for different modes. The results illustrate that the surface modes can be easily controlled and that the collective damping can be switched on and off conveniently.

ACKNOWLEDGMENTS

This research is supported by grants from the King Abdulaziz City for Science and Technology (KACST) the Qatar National Research Fund (QNRF) under an NPRP grant, the National Science Foundation of China (Grants No. 91021012 and No. 10904113), and the Foundation of the Ministry of Science and Technology (Grants No. 2007CB13201 and No. 2011CB922203) and RGC (HKBU202910) of HK Government. One of us (J.X.) gratefully acknowledges the hospitality at KACST, where most of this work was done.

[1] C. Bennett, Phys. Today **48**(10), 24 (1995).
[2] T. Yu and J. H. Eberly, Phys. Rev. Lett. **93**, 140404 (2004).
[3] J. H. Eberly and T. Yu, Science **316**, 555 (2007).
[4] D. Braun, Phys. Rev. Lett. **89**, 277901 (2002).
[5] A. Beige, S. Bose, D. Braun, S. F. Huelga, P. L. Knight, M. B. Plenio, and V. Vedral, J. Mod. Opt. **47**, 2583 (2000).
[6] L. Jakobczyk, J. Phys. A **35**, 6383 (2002).
[7] F. Benatti, R. Floreanini, and M. Piani, Phys. Rev. Lett. **91**, 070402 (2003).
[8] Z. Ficek and R. Tanas, Phys. Rev. A **77**, 054301 (2008).
[9] M. Paternostro, M. S. Tame, G. M. Palma, and M. S. Kim, Phys. Rev. A **74**, 052317 (2006).
[10] S. Natali and Z. Ficek, Phys. Rev. A **75**, 042307 (2007).
[11] Y. P. Yang, J. P. Xu, H. Chen, and S. Y. Zhu, Phys. Rev. A **82**, 030304(R) (2010).
[12] D. Dzsotjan, A. S. Sørensen, and M. Fleischhauer, Phys. Rev. B **82**, 075427 (2010).
[13] A. Gonzalez-Tudela, D. Martin-Cano, E. Moreno, L. Martin-Moreno, C. Tejedor, and F. J. Garcia-Vidal, Phys. Rev. Lett. **106**, 020501 (2011).
[14] R. H. Dicke, Phys. Rev. **93**, 99 (1954).
[15] R. H. Lehmberg, Phys. Rev. A **2**, 883 (1970).
[16] W. K. Wootters, Phys. Rev. Lett. **80**, 2245 (1998).
[17] H. T. Dung, L. Knoll, and D.-G. Welsch, Phys. Rev. A **66**, 063810 (2002).
[18] J. P. Xu, Y. P. Yang, and S. Y. Zhu, J. Mod. Opt. **57**, 1473 (2010).
[19] J. P. Xu, Y. P. Yang, Q. Lin, and S. Y. Zhu, Phys. Rev. A **79**, 043812 (2009).
[20] H. Raether, *Surface Plasmons on Smooth and Rough Surfaces and on Gratings* (Springer, Berlin, 1988).
[21] C. Girard, O. J. F. Martin, and A. Dereux, Phys. Rev. Lett. **75**, 3098 (1995).
[22] E. Dulkeith, A. C. Morteani, T. Niedereichholz, T. A. Klar, J. Feldmann, S. A. Levi, F. C. J. M. van Veggel, D. N. Reinhoudt, M. Möller, and D. I. Gittins, Phys. Rev. Lett. **89**, 203002 (2002).
[23] J. R. Lakowicz, Plasmonics **1**, 5 (2006).
[24] M. Ringler, A. Schwemer, M. Wunderlich, A. Nichtl, K. Kürzinger, T. A. Klar, and J. Feldmann, Phys. Rev. Lett. **100**, 203002 (2008).
[25] D. E. Chang, A. S. Sørensen, P. R. Hemmer, and M. D. Lukin, Phys. Rev. Lett. **97**, 053002 (2006).
[26] O. Kulakovich, N. Strekal, A. Yaroshevich, S. Maskevich, S. Gaponenko, I. Nabiev, U. Woggon, and M. Artemyev, Nano Lett. **2**, 1449 (2002).
[27] P. Vasa, R. Pomraenke, and S. Schwieger, Phys. Rev. Lett. **101**, 116801 (2008).
[28] M. Al-Amri and M. Babiker, Phys. Rev. A **67**, 043820 (2003).
[29] D. Martin-Cano, L. Martin-Moreno, F. J. Garcia-Vidal, and E. Moreno, Nano Lett. **10**, 3129 (2010).
[30] R. Ruppin, Phys. Lett. A **277**, 61 (2000).
[31] R. Ruppin, J. Phys. Condens. Matter **13**, 1811 (2001).
[32] V. G. Veselago, Sov. Phys. Usp. **10**, 509 (1968).
[33] D. Schurig, J. J. Mock, and D. R. Smith, Appl. Phys. Lett. **88**, 041109 (2006).
[34] S. Zhang, W. J. Fan, B. K. Minhas, A. Frauenglass, K. J. Malloy, and S. R. J. Brueck, Phys. Rev. Lett. **94**, 037402 (2005).
[35] H. J. Lezec, J. A. Dionne, and H. A. Atwater, Science **316**, 430 (2007).
[36] G. Dolling, M. Wegener, C. M. Soukoulis, and S. Linden, Opt. Lett. **32**, 53 (2007).
[37] P. B. Johnson and R. W. Christy, Phys. Rev. B **6**, 4370 (1972).
[38] M. S. Tomaš, Phys. Rev. A **51**, 2545 (1995).
[39] J. B. Pendry, Phys. Rev. Lett. **85**, 3966 (2000).
[40] R. Liu, C. Ji, J. J. Mock, J. Y. Chin, T. J. Cui, and D. R. Smith, Science **323**, 366 (2009).
[41] J. Kästel and M. Fleischhauer, Phys. Rev. A **71**, 011804(R) (2005).
[42] D. Chanda, K. Shigeta, S. Gupta, T. Cain, A. Carlson, A. Mihi, A. J. Baca, G. R. Bogart, P. Braun, and J. A. Rogers, Nat. Nanotechnol. **6**, 402 (2011).
[43] Y. Zhao, F. Chen, Q. Shen, Q. Liu, and L. Zhang, Opt. Express **19**, 11605 (2011).